LOCAL VELOCITY AND SHEAR DEFORMATION RATE AT MODEL MEMBRANES IMMERSED IN A BIOREACTOR AGITATED BY CURVED-BLADE IMPELLER: THE EFFECT OF MEMBRANE POSITION

Serafim Vlaev, Daniela Dzhonova-Atanasova

Institute of Chemical Engineering, Bulgarian Academy of Sciences,
"Acad. G. Bonchev" Str., Bl.103, 1113 Sofia, Bulgaria

Abstract

A stirred bioreactor equipped with two submerged tubular membrane modules and curved-blade, backswept (BS) impellers is studied. The membranes are positioned in different parts of the vessel, a subsurface and a bottom one. The flow conditions at the membranes for effective fouling control are targeted. Contemporary CFD methodology is applied. The zones of major importance for effective operation of the membranes are examined and the values of hydrodynamic parameters are revealed. In these zones, the local velocity and shear parameters' distributions are determined. The flow parameters are correlated with impeller rotational speed and fluid viscous properties. Angular velocity is varied between 600 and 1100 rpm and bulk viscosity is varied between 1 and 60 mPa s. The role of aeration is specified. The maximum shear rates at the membrane interface are registered. The corresponding stress force imposed by the BS impellers is compared with the one generated by conventional flat- blade Rushton turbine (RT). The hydrodynamic data are compared with reference data from the literature and the possibility for effective operation non-damaging for living micro-organisms is discussed.

Key words: *membrane technology, stirred bioreactors, modeling and simulation*

1. INTRODUCTION

Membrane separation is an important step in overall downstream processing of biological product materials. Advantage of the integrated bioreactor with membrane separation is its ability to separate products of different types with sufficient difference in molecular mass from complex systems with varying concentrations and composition. The integrated membrane reactors compete successfully with conventional continuous reactors with suspended biomass and agitation (Bakonyi et al. 2014), the submerged membrane bioreactor being of special interest (Mohammadmahdi et al. 2015, Jiang et al. 2016, Dosta et al. 2011). The latter includes creating conditions for high product quality at reduced energy consumption and reduced amounts of the solvents used (Martınez et al. 2012), as well as beneficial economic estimates such as lower operating costs of the integrated operation (Wei et al. 2014).

Essential progress is observed in integrated membrane systems that combine multiple membrane separation processes with different beneficial characteristics, integrated with a bioreactor, e.g.: forward osmosis and microfiltration (FO-MF) (Luo et al. 2015), membrane distillation (FO-MD) (Wang et al. 2015), reverse osmosis (FO-RO)(Goh et al. 2016), pressure retarded osmosis (FO-PRO, RO-PRO) (Goh et al. 2016, Eyvaz et al. 2016), etc.

Membrane modules immersed in the bioreactor, or side stream ones connected in recycle have been used in different biotechnological processes for separation of thermally unstable products. They have proven their efficiency in biological treatment of waste flows with high content and variety of organic contaminants, as well as an effective barrier against many active pharmaceutical ingredients, pesticides, alkylphenols from production of nonionic surfactants and other endocrine disrupters and resistant to degradation organic pollutants (Peeva et al. 2014, Tambosi et al. 2010, Nguyen et al. 2013). The design of this type of integrated reactors is the subject of further analysis and classification for: Biofuels production (Wei et al. 2014, Teixeira et al. 2014, Abels et al. 2013) for separating the products of the trans-esterification; Separation of carboxylic acids from industrial fermentation (López-Garzón et al. 2014, Lubsungneon et al. 2014, Ghaffar et al. 2014); Separation of amino acids and peptides - e.g. of L-glutamic acid from the fermentation broth by a sequence of membranes (Kumar et al. 2014); p-

nonylphenol removal under nitrifying conditions (Buitrón et al. 2015) in submerged membrane bioreactor using tubular membrane module.

The engineering part of the reactor design including membrane separation, its optimal geometry and conditions for the integrated process (Andrić et al. 2010) have been the subject of considerable scientific interest. Mathematical models of various complexity (Dey et al. 2013, Naessens et al. 2012) have been employed, accounting for the interrelationship between biokinetics, filtration and hydrodynamics of the integrated system. In recent years, an increasing interest in CFD modeling of integrated processes is observed (Naessens et al. 2012, Jalilvand et al. 2014), as well as models of integrated economic calculations (Naessens et al. 2012).

Recent developments in membrane separation technology and increased implementation of various membrane techniques for water purification and recovery of value added products bring attention to the lack of data on the performance of membranes designed as immersed modular systems in stirred tanks (Brannock et al. 2009) The impellers generate rigorous mixing and high rates of circulation around membranes and thus are potentially good turbulence promoters what is a desirable condition in view of the membrane fouling control. Combined knowledge on the performance of the integrated systems, based on the fluid flow in stirred tank reactors and the separation dynamics of immersed membranes, is needed. At condition of negligible effect of permeation on the hydrodynamic conditions at the membrane surface, the impeller-induced cross flow was examined (Vlaev & Tsibranska 2015). In the CFD simulations, the rate-of-deformation tensor was targeted, as determined by the local gradients of the component velocities near the membrane interface (Vlaev & Tsibranska 2015). CFD was applied to demonstrate the effect of reactor configurations (the relative position between membrane and impeller, effect of impeller design) on the fluid flow pattern in submerged membrane reactors (Meng et al. 2013). Modeling and characterization of bioreactor environments from mixing and shear perspectives at both small and large scales demonstrated high level of interest (Heath & Kiss 2007, Heidemann et al. 2014) with focus on traditional bioreactors with further analyses on integrated designs to be performed in such stirring vessels.

Controlled hydrodynamic conditions in the vicinity of the membrane surface are crucial for the flux stability, as well as in minimizing the membrane area requirement (Böhm et al. 2012) Enhancement of membrane shear-rates is considered as one of the most efficient factors for fouling control. Shear forces generated by pumps, bubbling or impellers are used to remove the fouling layer (Fane 2008). Yet care has to be taken for shear sensitive ingredients that may undergo deactivation (Menniti et al. 2009). From this point of view, the shear stress field and the homogeneity of the shear environment near the membrane surface have to be revealed.

One of the most efficient strategies to limit fouling is the use of a gas/liquid two-phase flow to enhance the mass transfer, the submerged membrane bioreactors being of special interest (Braak et al. 2011). Local Sherwood numbers and shear stress distributions at the membrane surface around bubbles at different gas velocities were approached by CFD simulations (Yang 2013). Optimum operation conditions for membrane modules, submerged in an aerated bioreactor, are searched (Wibisono et al. 2014) in direction of: positioning of the membrane modules, gas/liquid ratio, bubble size, trans-membrane pressure, obtaining sufficient wall shear stress to create friction on the membrane surface, impeller design and flow configuration. The discussion has to be made in view of uniformity of shear and velocity distributions in the volume of the reactor and along the membrane surface. Our preliminary results with CFD simulations of two-phase flow using Euler-Euler multiphase model shows that the distribution in gas presence is largely different, being more uniform (Vlaev et al. 2016). Further studies at different mixing impeller speeds and relative volumetric gas flow are needed.

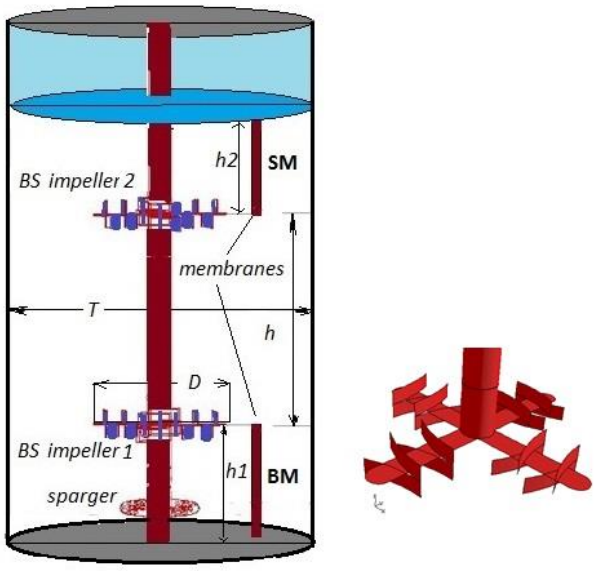
The aim of this study is to retrieve data on the flow field and fluid dynamic parameters, e.g. velocity components and gradients at membranes immersed in a bioreactor equipped with a modified curved blade impeller focusing also on the membrane position and the effect of the agitation by the specially designed impeller.

2. EXPERIMENTAL

The following experimental setup was subject to simulation studies. A 5l bioreactor (type Braun, Biotech) (Tisu & Pavko 2010) was used, as shown in Fig.1a schematic and Fig. 2. The vessel components' size were chosen to correspond to a design configuration used in real experiments aimed at polysaccharide exo-glucomannan production by yeast *Sporobolomyces salmonicolor* (Vlaev et al. 2013): The inner tank diameter was T=0.160 m, the overall liquid height was H=0.224 m and the distances between the impellers, the off bottom and the subsurface ones indicated in Fig. 1 were h=0.11 m, h_1=0.057 m, h_2=0.057 m, respectively. Two tubular modules, were positioned upside and downside, 59.5 mm long as shown and sized in the figure and marked as subsurface (SM) and bottom (BM) membrane units. The dual impeller design of the bioreactor included backswept arch-blade turbines with a diameter D=0.068 mm adopted by reference from previous studies (Kraitschev et al. 2000). The specific impeller design is shown in Fig. 1b and the particular size ratios are discussed in the reference paper (Kraitschev et al. 2000).

Gassed and non-gas operation was studied. Air was dispersed through a ring sparger with diameter 60 mm with twelve 1 mm-holes. Both impeller speed N and gas flow rate were identical with the real range of operational parameters practiced, e.g. 600-1100 rpm and 4.5 dm^3/min, respectively, the latter corresponding to volume-relative velocity of 1vvm (Vlaev et al. 2013).

Prototype power law fluids corresponding to different states of the experimental biofluid in Vlaev et al. (2013) were simulated, the flow index n and consistency coefficient K varying as follows: n=0.78, K=0.02 Pa.s^n, and n=0.78, K=0.1 Pa.s^n. The Metzner constant required to calculate the average shear rate for curved blades was 7.1 as reported by Taniyama & Sato (1965) and Nagata (1975). Bulk apparent viscosity range up to 64 mPa.s was covered. The flow pattern in small vessels is intensive one and the corresponding Reynolds numbers for rotational flow of 0.1-2.10^4 obtained assume turbulent conditions, the more so in impeller vicinity of located membranes.



a b

Fig. 1. Scheme of the simulated bioreactor with submerged tubular membrane modules. (a) Bioreactor, (b) Curved-blade backswept (BS) impeller used.

3. MODEL AND SIMULATION DETAILS

The cross-flow velocity and the velocity gradient at the membrane surface were determined by numerical procedure using CFD model and solution methodology of ANSYS Fluent R13.0. The following details were worked out.

The geometry is based on the configuration of the described integrated membrane bioreactor, Figs. 1 and 2, used in experimental studies (Vlaev et al. 2013).

The flow field was simulated by the RANS standard k-ε (SKE) model and the Eu-Eu formulation of two-phase gas-liquid flow. For the rotating volume the multiple reference frame (MRF) approach (Ferziger & Peric 1997) was used.

In ANSYS Fluent's implementation of the MRF model, the calculation domain is divided into subdomains, each of which rotating with respect to the laboratory (inertial) frame (ANSYS Fluent R13.0 2010). The present geometry, which includes two rotating impellers, is modeled using separate moving reference frames for the two impellers and separate stationary frames for the two membranes, the tank zone and the sparger. The cells of the tank zone are hexahedral, while the cells of the subdomains around the air sparger and the membrane tubes are tetrahedral allowing mesh refinement near the walls. Conformal mesh was formed in 6 volume zones, Fig. 3, with a total cell number of ca. 10^6. The MRF model enables steady state solution for the case without aeration.



Fig. 2. Bioreactor with BS impellers.

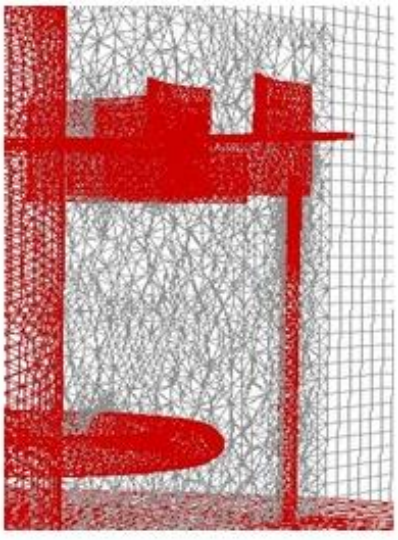


Fig. 3. Meshing of the multizone calculation domain.

The turbulent flow in a 3D domain was represented by Reynolds-Averaged Navier–Stokes (RANS) equations of continuity and momentum and closed by standard "k-ε"(SKE) model of turbulence (ANSYS Fluent R13.0 2010, Ranade 2002):

Equation of continuity:

$$(\rho u_i) = 0 \qquad (1)$$

Equation of momentum:

$$\frac{\partial}{\partial t}(\rho u_i) + \frac{\partial}{\partial x_j}(\rho u_i u_j) = -\frac{\partial p}{\partial x_i} + \frac{\partial}{\partial x_j}\left[\mu\left(\frac{\partial u_i}{\partial x_j} + \frac{\partial u_j}{\partial x_i} - \frac{2}{3}\delta_{ij}\frac{\partial u_k}{\partial x_k}\right)\right] + \frac{\partial}{\partial x_j}\left(-\rho\overline{u_i' u_j'}\right), \qquad (2)$$

where u_i indicates time-averaged velocity component, p is pressure, ρ is liquid density, μ is liquid dynamic viscosity.

The model liquid is non-Newtonian pseudo plastic (shear thinning) fluid. In this case μ is the non-Newtonian apparent viscosity, described by a power law:

$$\mu = K\dot{S}^{n-1}, \quad (3)$$

where K is consistency coefficient, n is flow index (n<1 for pseudo plastic fluids), $\dot{S}$ is the shear rate calculated as:

$$\dot{S} = \frac{\partial u_i}{\partial x_j} + \frac{\partial u_j}{\partial x_i}. \quad (4)$$

The shear stress τ is expressed as

$$\tau = K\dot{S}^n. \quad (5)$$

The effect of turbulence is represented by the term of the Reynolds stress, $-\rho\overline{u_i'u_j'}$, which is modelled by the equation:

$$-\rho\,\overline{u_i'u_j'} = \mu_t\left(\frac{\partial u_i}{\partial x_j} + \frac{\partial u_j}{\partial x_i}\right) - \frac{2}{3}\left(\rho k + \mu_t\frac{\partial u_k}{\partial x_k}\right)\delta_{ij}, \quad (6)$$

where k is turbulent kinetic energy,

μ_t is turbulent viscosity, calculated by

$$\mu_t = \rho C_\mu \frac{k^2}{\varepsilon}. \quad (7)$$

Here ε is the dissipation rate and $C\mu$ is a constant.

The transport equations of k and ε are:

$$\frac{\partial}{\partial t}(\rho k) + \frac{\partial}{\partial x_i}(\rho k u_i) = \frac{\partial}{\partial x_j}\left[\left(\mu + \frac{\mu_t}{\sigma_k}\right)\frac{\partial k}{\partial x_j}\right] + G_k - \rho\varepsilon, \quad (8)$$

$$\frac{\partial}{\partial t}(\rho \varepsilon) + \frac{\partial}{\partial x_i}(\rho \varepsilon u_i) = \frac{\partial}{\partial x_j}\left[\left(\mu + \frac{\mu_t}{\sigma_\varepsilon}\right)\frac{\partial \varepsilon}{\partial x_j}\right] + C_{1\varepsilon}\frac{\varepsilon}{k}G_k - C_{2\varepsilon}\rho\frac{\varepsilon^2}{k}, \quad (9)$$

where G_k represents the generation of turbulence kinetic energy due to the mean velocity gradients, calculated as

$$G_k = -\rho\overline{u_i'u_j'}\frac{\partial u_j}{\partial x_i}.$$

$C_{1\varepsilon}$ and $C_{2\varepsilon}$ are constants and σ_k and σ_ε are the turbulent Prandtl numbers for k and ε.

The presence of gas in the two-phase flow case is modeled by the Euler-Euler formulation, which allows for the modeling of two separate, yet interacting phases (ANSYS Fluent R13.0 2010). An Eulerian treatment is used for each phase. A single pressure is shared by the two phases. The description of the two-phase flow as interpenetrating continua incorporates the concept of phasic volume fractions. They represent the space occupied by each phase, and the laws of conservation of mass and momentum are satisfied by each phase individually. For the air flow a unique bubble size of 2 mm was assumed (in order to reduce the computational demands). Momentum and continuity equations, as well as transport equations for k and ε, are solved for each phase. The equations are solved using finite volume technique.

The following boundary conditions are specified: velocity inlet at the air inlet; pressure outlet at the free surface of the reactor; no-slip conditions at the solid surfaces including the membrane walls, where no-permeation is assumed.

The rate-of-deformation tensor (as determined by the local gradients of the component velocities near the membrane interface) and the averaged over the membrane surfaces shear stresses are targeted in the simulations compared to measurements of the wall shear rate via the electro-diffusion method using a spherical probe adjacent to the membrane tip (Vlaev et al. 2006).

4. RESULTS AND DISCUSSION

Both fluid shear rate and membrane surface wall shear were target values and the vessel bulk and membrane surface were examined. The flow field is presented in mid-vessel vertical plane passing through the membrane and X-Y plots along radial central lines in the planes of the impellers passing through the membrane tip, Fig. 4. The results are represented in tank scale and membrane scale (Fig. 5). Aimed at bulk and membrane surface shear conditions, corresponding volume-averaged, surface-averaged and maximum parameter values were determined.

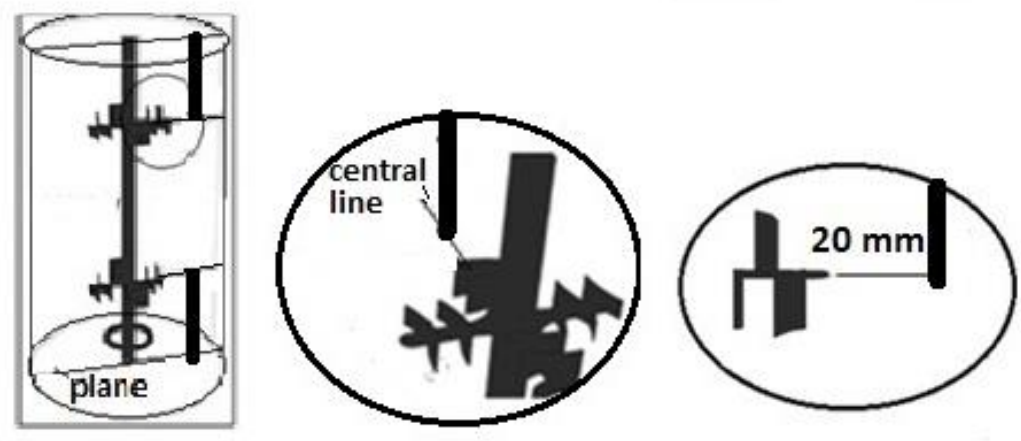


Fig. 4. Scheme of mid-vessel plane and radial line of results' presentation.

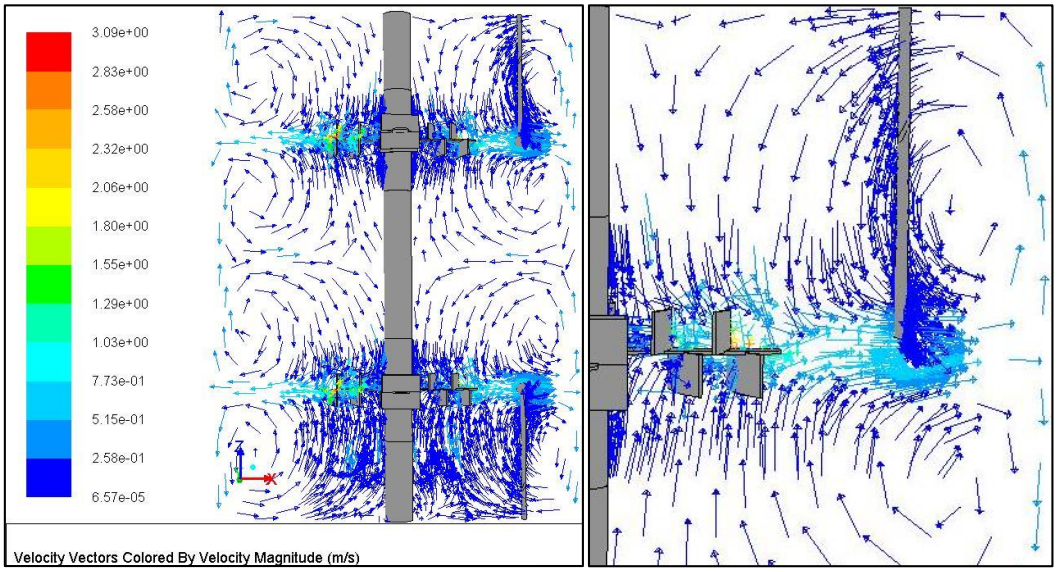


Fig. 5. Flow pattern of the BS impellers in the mid-vessel plane and in the vicinity of the immersed model membrane (SM), 900 rpm.

The flow pattern was studied at various operational conditions resembling a real process in the bioreactor. Fig. 5 shows typical 2D-image of the flow field, the velocity vectors, their magnitude in a coloured scale. It correspond to impeller speed of 900 rpm and illustrates the characteristic non-uniform velocity distribution. The highest fluid velocity occurs near the impeller tips. Along the blade discharge, velocity decreases and a flow swirl in axial direction is seen. In its way, such pattern creates tangetial flow near the membrane walls as a favourable and most efficient condition for fouling mitigation. At

the particular impeller speed, the problematic zones of low velocity are small. However, considering cell living conditions the maximum velocity corresponding to tip velocity $v^*=\pi ND$=3.2 m/s is higher than the critical value of 1-2 m/s proposed in literature (Eibl & Eibl 2009) as the maximum tolerable fluid velocity for mammalian cells. This means that zones with intolerably high velocity for the cells might appear at this rpm.

Model validation has been carried out in a separate study in a 50L stirred bioreactor by comparing area-averaged shear rate data at membrane surfaces with wall shear rate values determined by the electro-diffusion method using a spherical probe adjacent to a similar membrane tip. The experiments have been described in detail elsewhere (Vlaev et al. 2006). Two types of impellers were studied, RT and curved-blade Narcissus (NS) impeller. In that work, the same RANS SKE simulations with similar assumptions were evaluated and assessed. The reported predicted and measured shear rate values compared well within a maximum relative deviation of 17 %.

Figs. 6-11 illustrate the shear field variation relationships.

The effect of non-Newtonian properties upon average shear rate is illustrated in Fig. 6 and 7 and a data summary is presented in Table 1. High apparent viscosity of the non-Newtonian fluid (e.g. the case of K=0.1 mPa.s^n, n=0.78) is found to decrease the fluid mobility and to increase the problematic zones of low mixing, which is evident from the lower values of the bulk and surface shear rates, Figs. 6 and 7, but leads to higher wall shear stresses compared to low-viscosity fluid, Table 1.

Considering the effect of rpm, higher rpm, on the contrary, is found to increase the bulk and surface shear rates. The BS flow average shear rates determined for regimes of 600-1100 rpm, are less than 55 1/s in the bulk, Fig. 6, and less than 1700 at the membrane surfaces, Fig. 7. However, unlimited impeller speed rise is not practical, as the higher velocity gradients lead to maximum shear rate values of the order of 10^2 1/ks that may exceed the critical ones reported in literature. For reference, values of 1–3x10^5 1/s have been reported (Chisti 2001) to damage animal cells irrevercibly. Yet the effect of the high maximum values is restricted to very small volume fractions, as seen in the histograms of shear distribution, Fig. 11. Further studies are needed to assess the risk of cell damage.

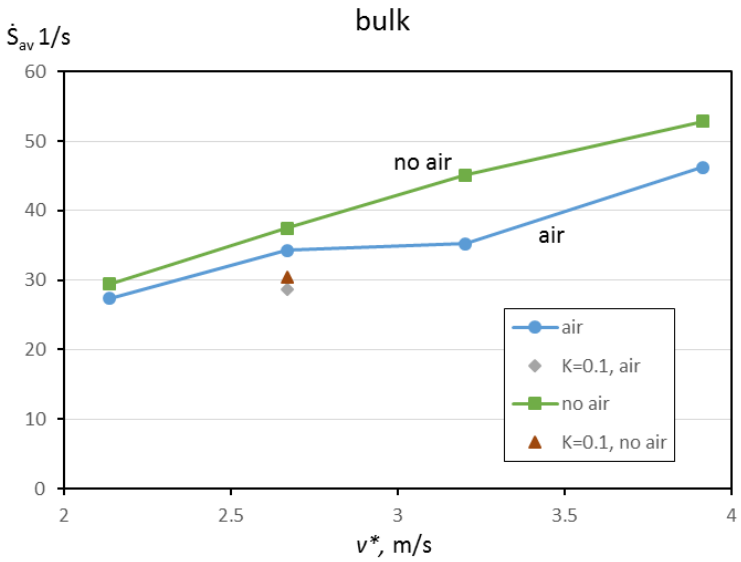


Fig. 6. Volume-averaged shear rate in the tank, 600-1100 rpm.

The effect of aeration has been studied. The aeration at flow rates typical for bioreactors does not change substantially the flow pattern in the bulk. Nevertheless in gas presence there is a shear rate drop of up to 30% in the bulk area and in the area of membrane-liquid interface, Fig. 6 and 7.

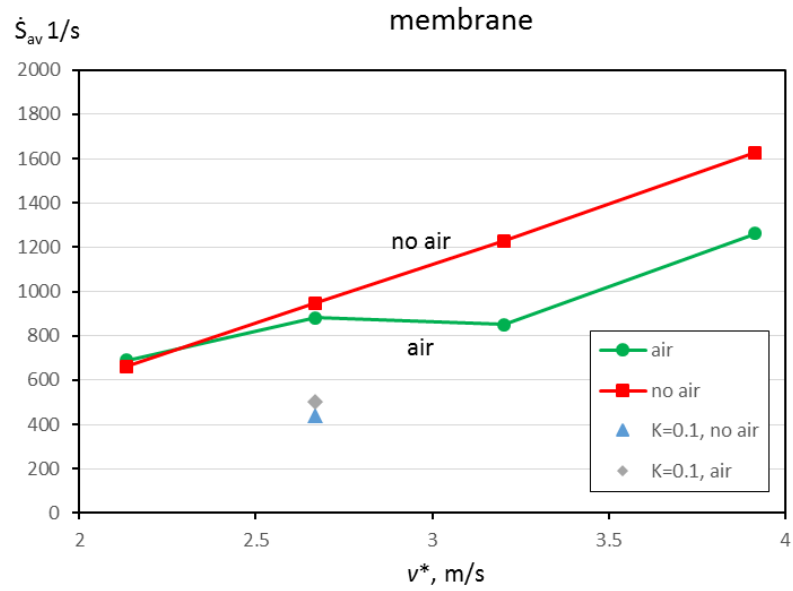


Fig. 7. Surface-averaged shear rates based on the total surface of the two membrane modules, 600-1100 rpm.

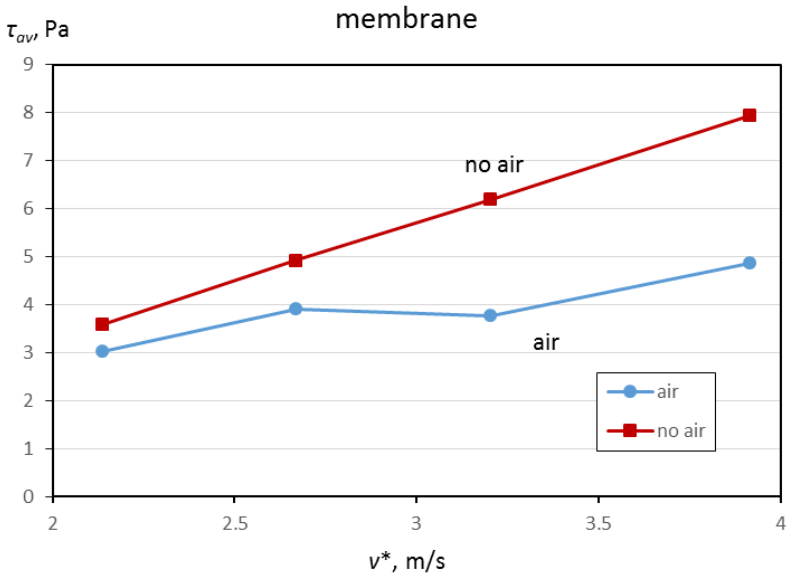
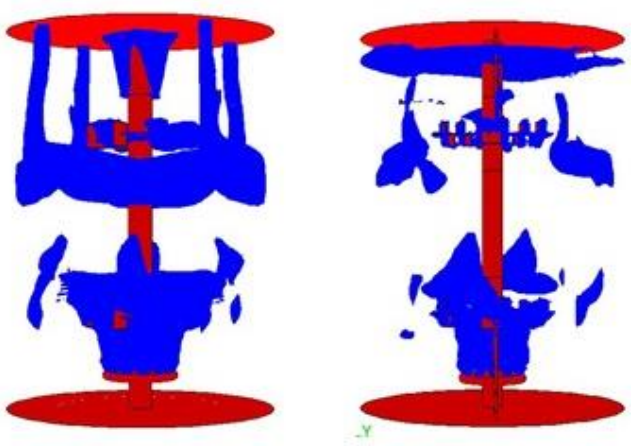


Fig. 8. Surface-averaged wall shear stress values based on the total surface of the two membrane modules, 600-1100 rpm.

The shear decrease can be explained with the decrease in impeller power draw in gas presence and change of the flow structure, due to the tendency of the air to propagate around the impellers, which hinders the mixing at higher rpm. The effect seems to be a strong one for the case of impeller BS. Fig. 9 contains a background illustration to confirm this observation showing iso-surface of 10 % gas hold-up for two impellers, e.g. the BS impeller and the radial flow RT one. It is noteworthy that the sparger position leads to central and peripheral gas hold-up zones in the RT case and predominantly central gas hold-up zones around the impellers in the BS case. Consequently, the different structure of gas dispersion influences the shear force.



a b

Fig. 9. Iso-surfaces of gas hold-up 10% in a stirred reactor compared at close values of specific input power: RT impellers 400 rpm, b) BS impellers 750 rpm.

Apart from shear average values, shear distribution is important parameter. Fig. 10 shows shear rate distribution along the radial lines passing at the impellers' level through the membrane module tips. The effect of air flow is seen as a slight rise in the shear rate at the SM surface and a decrease at the BM one.

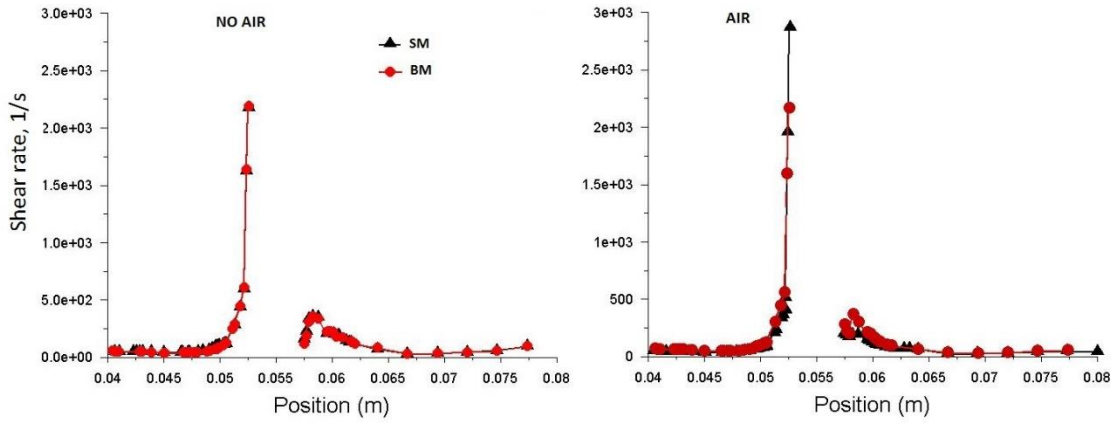


Fig. 10. Shear rate distribution along the radial central line in impeller planes passing through the tip of membrane SM and BM, 750 rpm.

Changes in shear distribution along membrane surface related to membrane position have been observed. These are seen best by histograms. The shear rate distribution, as given in Fig.11, was obtained by discretizing the shear rate values into 250 bins and summing up the number of cells, where the shear rate occurred. The histograms in Fig. 11 reveal some difference in frequency distribution of shear rates on the surface of the two membranes, i.e. SM and BM. Yet the values of maximum frequency for the membranes are close ones. About shear rate value of 150 1/s, the frequency distribution function shows maximum frequency of about 2.7 % for SM and about 3.9% for BM. Both membrane modules were found to show close maximum shear rate values of about 7 1/ks (cf Table 1).

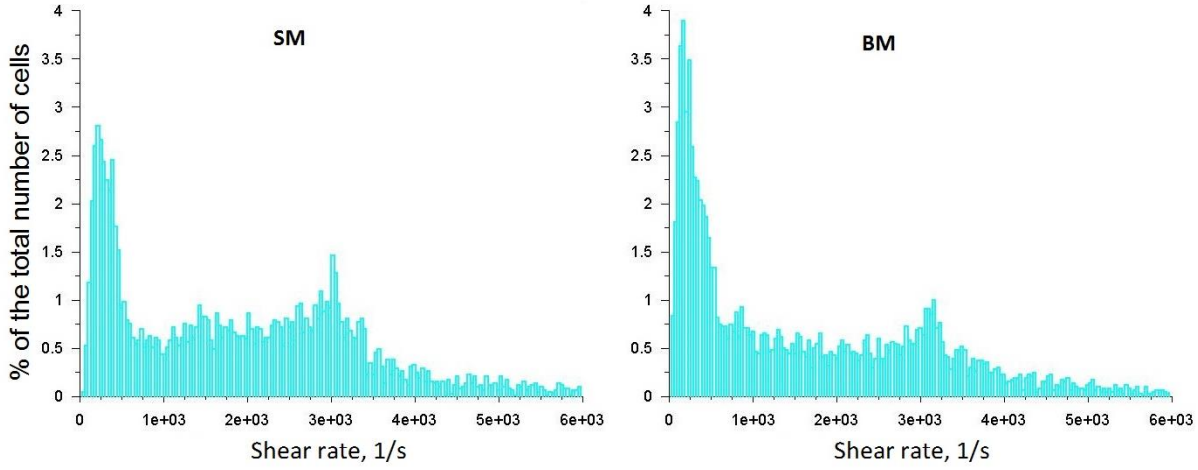


Fig. 11. Frequency distribution of membrane shear rate at 750 rpm in the aeration case.

Table 1 presents a summary on the shear results obtained, with the shear stress values determined. In the table, the bottom and subsurface membranes, i.e. BM and SM data, are compared. One could see the difference of BM and SM shear data at non-gassed and gassed conditions, seen as higher shear rate (17-26%) for the subsurface membrane at aeration and the opposite effect (3-5%) in gas absence. With reference to the data on gas volume fraction at the membrane-fluid interface shown in column 3, one can see that the accumulation of gas in the vessel upper section e.g. 27-55% near SM compared to 3-6% near the BM, is likely to be the reason, as the gas spread leads to velocity gradient rise and explains the above difference at aeration. As the shear stress depends also on the membrane-liquid contact area and the increase in gas volume fraction leads to liquid contact area decrease, the final effect in gas presence upon the shear stress is leveled and the effect at the subsurface membrane is diminished. Because fouling mitigation depends on shear force, the higher shear force per unit surface area at the subsurface position is noteworthy and the fouling control there is likely to be more efficient. This should be the preferred location for risky separation media. Beyond the issue of position, shear stress values in the range 1-6 Pa have been reported (Koutsou & Karabelas 2012) to ensure good performance of membranes in terms of fouling control and concentration polarization in both positions. Comparing the membrane performance data of this study, the shear force values determined for the BS flow bioreactor could be considered acceptable for fouling mitigation.

Table 1. Shear rate and shear stress at membrane surface for BS impellers in two positions

Fluid *n/K*	*N*, rpm	Gas volume fraction at BM/SM	Re x10^3 at membrane	μ_{av}, mPa s at membrane	$\dot{S}_{max}$, 1/ks at membrane	$\dot{S}_{av}$, 1/s at BM/SM	τ_{av}, Pa at BM/SM
0.78/0.02	600	0	8.9	5.5	5.3	679/647	3.65/3.5
		0.03/0.55	8.2	6.0	4.9	659/804	3.3/3.02
0.78/0.02	750	0	7.7	8.0	7.3	964/932	5.0/4.8
		0.06/0.27	6.1	10.0	7.3	830/1045	3.9/4.3
0.78/0.02	900	0	15.3	4.8	9.6	1252/1204	6.3/6.1
		0.06/0.32	13.6	5.4	6.9	823/981	3.9/4.1
0.78/0.02	1100	0	19.9	4.5	12.8	1656/1600	8.1/7.8
		0.17/0.36	19.0	4.7	11.2	1448/1206	5.6/4.7
0.78/0.1	750	0	1.9	32	3.4	437/437	10.8/10.8
		0.1/0.14	1.3	45	3.7	492/576	46.8/55.6

μ_{av}- surface-averaged apparent viscosity

Furthermore, the shear data determined in this study for the membrane exposed to backswept cross-flow was compared with reference data determined for similar membrane exposed to flat-blade radial flow (Vlaev et al. 2016, Vlaev & Tsibranska 2015) based on similar level of specific power input. Comparing cases of low apparent viscosity (~6 mPa.s, n=0.78, K=0.02 mPa.s^n), the BS case at 600 rpm (1.7 W/dm^3) generated $\dot{S}_{av}$=663 1/s compared to 1330 1/s in the case RT at 400 rpm at similar specific power input (1.5 W/dm^3). Comparing cases of high viscosity (~35 mPa.s, n=0.78, K=0.1 mPa.s^n), the BS case at 750 rpm (8.6 W/dm^3) generated $\dot{S}_{av}$=437 1/s compared to 3600 1/s in the RT case at 750 rpm at similar specific power input (7.7 W/dm^3). Both flow configurations showed acceptable turbulence promotion for fouling mitigation. However, considering the criteria for hindered shear influence upon shear-sensitive cells, the positive effect of the backswept impeller flow characteristic is seen, as lower shear stress of up to 8 Pa in the configuration of this study against shear stress of up to 59 Pa in the RT vessel, shear stress exceeding 30-40 Pa being reported as harmful (Neunstoeklin et al. 2015).

5. CONCLUSIONS

High apparent viscosity and deviation from Newtonian flow decrease liquid mobility and increase the regions with low shear rate in the liquid bulk but tend to increase the wall shear stress at the membranes.

High impeller speed increases the shear rates and is likely to reduce the membrane fouling, the average shear rate values being far below the critical values of cell damage for all the rpm studied.

Air sparging, which is known to improve mixing and helps to prevent membrane fouling, has been found to cause negative effect upon the bulk and membrane shear rate, due to dependencies on the flow structure by the gas hold-up.

Referring to the effect of membrane position in terms of fouling prevention, the average shear stress data suggests high performance in both positions of the submerged membrane modules for all regimes of the BS flow configuration studied. Stronger positive effect has been registered for the bottom module in single-phase flow, while the effect may be diverse in the presence of gas and in concentrated solutions

ACKNOWLEDGEMENT

This work is supported by the National Science Fund - Ministry of Education and Science, Contract DN 07/11-15.12.2016.

REFERENCES

Abels, C, Carstensen, F, Wessling, M 2013, Membrane processes in biorefinery applications, *Journal of Membrane Science* 444, pp. 285–317.

Andrić, P, Meyer, AS, Jensen, PA, Dam-Johansen, K 2010, Reactor design for minimizing product inhibition during enzymatic lignocellulose hydrolysis II. Quantification of inhibition and suitability of membrane reactors, *Biotechnology Advances* 28, pp. 407–425.

ANSYS Fluent R13.0 2010, *Documentation*.

Bakonyi, P, Nemestóthy N, Simon V, Bélafi-Bakó K 2014, Fermentative hydrogen production in anaerobic membrane bioreactors: A review, *Bioresource Technology* 156, pp.357–363.

Böhm, L, Drews, A, Prieske, H, Bérubé, PR, Kraume, M 2012, The Importance of Fluid Dynamics for MBR Fouling Mitigation, *Bioresource Technology*, vol. 122, p. 50.

Braak, E, Alliet, M, Schetrite, S, Albasi, C 2011, Aeration and hydrodynamics in submerged membrane bioreactors, *Journal of Membrane Science*, vol. 379, no. 1, pp. 1-18.

Brannock, MWD, De Wever, H, Wang, Y, Leslie, G 2009, CFD Simulations of MBRs: Inside submerged versus outside submerged membranes. *Desalination*, 236, pp. 244-251.

Buitrón, G, Torres-Bojorges, A X, & Cea-Barcia, G 2015, Removal of p-nonylphenol isomers using nitrifying sludge in a membrane sequencing batch reactor, *Chemical Engineering Journal*, 281, pp. 860-868.

Dey, P, Pal, P 2013, Modelling and simulation of continuous L (+) lactic acid production from sugarcane juice in membrane integrated hybrid-reactor system, *Biochemical Engineering Journal* 79, pp. 15– 24.

Dosta J,. Nieto JM, Vila J, Grifoll, M, Mata-Álvarez, J 2011, Phenol removal from hypersaline wastewaters in a Membrane Biological Reactor (MBR): operation and microbiological characterisation. Bioresource technology, vol. 102, no. 5, pp.4013-4020.

Eibl, R, Eibl, D 2009, Application of disposable bag bioreactors in tissue engineering and for the production of therapeutic agents. In: Kasper C, Griensven M, Pörtner R (eds) Bioreactor systems for tissue engineering. Springer, Berlin.

Eyvaz, M, Aslan, T, Arslan, S, Yüksel, E, Koyuncu, I 2016, Recent developments in forward osmosis membrane bioreactors: a comprehensive review. *Desalination and Water Treatment*, pp.1-36.

Fane, AG 2008, Submerged Membranes, *Ch. 10, in* Li, NN, Fane, AG, Winston-Ho, WS, Matsuura, T, *Advanced Membrane Technology and Applications*, New Jersey: Wiley, p. 239.

Ferziger, JH, Peric, M 1997, *Computational methods for fluid dynamics*, Springer.

Georgiev, D., Vlaev, S 2015, Investigation of the flow pattern of a curved- blade impeller for application in bioreactors with shear sensitive organisms, Research publications of University of Ruse, Vol. 54, no 10.2, pp. 195-199 (in Bulg.)

Ghaffar ,T, Irshad, M, Anwar, Z, Aqil, T, Zulifqar, Z, Tariq, A, Kamran, M, Ehsan, N, Mehmood, S 2014, Recent trends in lactic acid biotechnology: A brief review on production to purification, *Journal of Radiation Research and Applied Sciences*, 7, pp. 222-229.

Goh, PS, Matsuura, T, Ismail, AF, Hilal, N 2016, Recent trends in membranes and membrane processes for desalination. *Desalination*, 391, pp. 43-60.

Heath, C, Kiss, R 2007, Cell culture process development: Advances in Process Design, *Biotechnol. Progr.*, 23, pp. 46-51.

Heidemann, R, Cruz, CR et al. 2014, Single-use bioreactors for the rapid production of preclinical and clinical biopharmaceuticals, *Biopharm International*, 27, pp. 22-34.

Jalilvand, Z, Ashtiani, FZ, Fouladitajar, A, Rezaei, H 2014, Computational fluid dynamics modeling and experimental study of continuous and pulsatile flow in flat sheet microfiltration membranes, *Journal of Membrane Science* 450, pp. 207–214.

Jiang, H, Qu, Z, Li, Y, Huang, J, Chen, R, Xing, W 2016, One-step semi-continuous cyclohexanone production via hydrogenation of phenol in a submerged ceramic membrane reactor, *Chemical Engineering Journal*, 284, pp. 724-732.

Kraitschev, S, Vlaev, SD, Lossev, V, Staykov, P 2000, A new arc-blade version of a turbine impeller suitable for bioreactors, *Biotechnol. & Biotechnol. Eq.*, 15, pp. 128-131.

Koutsou, CP, & Karabelas, AJ 2012, Shear stresses and mass transfer at the base of a stirred filtration cell and corresponding conditions in narrow channels with spacers, *J. Membrane Sci.*, 399-400, pp. 60-72.

Kumar, R, Vikramachakravarthi, D, Pal, P 2014, Production and purification of glutamic acid: A critical reviewtowards process intensification, *Chemical Engineering and Processing* 81, pp. 59–71.

López-Garzón, CS, Straathof, AJJ 2014, Recovery of carboxylic acids produced by fermentation, *Biotechnology Advances* vol. 32, no.5, pp.873-904.

Lubsungneon, J, Srisuno, S, Rodtong, S, Boontawan, A 2014, Nanofiltration coupled with vapor permeation-assisted esterification as an effective purification step for fermentation-derived succinic acid, *Journal of Membrane Science*, 459, pp. 132–142.

Luo, W, Hai, FI, Kang, J, Price, WE, Nghiem, LD, Elimelech, M 2015, The role of forward osmosis and microfiltration in an integrated osmotic-microfiltration membrane bioreactor system, Chemosphere, 136, pp.125-132.

Martınez, MB, Van der Bruggen, B, Negrin, ZR, Alconero, PL 2012, Separation of a high-value pharmaceutical compound from waste ethanol by nanofiltration, *Journal of Industrial and Engineering Chemistry*, vol. 18, pp.1635–1641.

Meng, L, Cheng, J C., Jiang, H, Yang, C, Xing, WH, & Jin, WQ 2013, Design and analysis of a submerged membrane reactor by CFD simulation, *Chemical Engineering & Technology*, vol. 36, no. 11, pp.1874-1882.

Menniti, A, Kang, S, Elimelech, M, Morgenroth, E 2009, Influence of Shear on Production of Extracellular Polymeric Substances in Membrane Bioreactors, *Water Research*, vol. 43, p. 4305.

Mohammadmahdi, M, Stickel, J, Wickramasinghe, SR 2015, Investigation of a submerged membrane reactor for continuous biomass hydrolysis, *Food and Bioproducts Processing* 96, pp. 189-197.

Naessens, W, Maere, T, Ratkovich, N, Vedantam, S, Nopens, I 2012, Critical review of membrane bioreactor models – Part 2: Hydrodynamic and integrated models, *Bioresource Technology* 122, pp. 107–118.

Nagata, S 1975, *Mixing Principles and Applications*, Wiley, New York.

Neunstoecklin, B, Stettler, M, Solacroup, Th, Broly,H, Morbidelli, M, Soos, M 2015, Determination of the maximum operating range of hydrodynamic stress in mammalian cell culture, *J. Biotechnol*., 194, pp.100-109.

Nguyen LN, Hai, FI, Kang, J, Price WE, Nghiem LD 2013, Removal of emerging trace organic contaminants by MBR-based hybrid treatment processes, *International Biodeterioration & Biodegradation* 85, pp. 474-482.

Peeva, L, da Silva Burgal, J, Valtcheva, I, Livingston AG 2014, Continuous purification of active pharmaceutical ingredients using multistage organic solvent nanofiltration membrane cascade, *Chemical Engineering Science*, 116, pp. 183–194.

Ranade, VV 2002, *Computational flow modeling for chemical reactor engineering*, Academic Press, London.

Tambosi, J, de Sena, R, Favier, M, Gebhardt, W, José, H, Schröder, H, Moreira, R 2010, Removal of pharmaceutical compounds in membrane bioreactors (MBR) applying submerged membranes, *Desalination* 261,pp. 148–156.

Taniyama, I, Sato, T 1965, *Kagaku Kogaku (Chem. Eng., Japan)*, 29, p.709.

Teixeira, CB, Madeira Junior, JV, Macedo, GA 2014, Biocatalysis combined with physical technologies for development of a green biodiesel process, *Renewable and Sustainable Energy Reviews* 33, pp. 333–343.

Tisu, M, Pavko, A 2010, Oxygen transfer in a laboratory STR during mammalian cell culture cultivation, *Acta Chim. Slov*. 57, pp. 123-128.

Vlaev SD, Nikov, I, Martinov, M 2006, Shear and scin friction on particles in power-low fluids agitated by flat-blade and fluid foil impellers, *Chemical Engineering and Science* 61, pp. 5455-5467.

Vlaev, S, Rusinova-Videva, S, Pavlova, K, Kuncheva, M, Panchev, I, Dobreva, S 2013, Submerged culture process for biomass and exopolysaccharide production by Antarctic yeast: some engineering considerations. *Appl. Microbiol. Biotechnol*., vol. 97no. 12, pp. 5303-13.

Vlaev SD, Tsibranska, I 2015, Shear stress generated by radial flow impellers at bioreactor-integrated membranes, *Proceedings of the 15th European Conference on Mixing (28.06.-3.07.2015)*, St. Peterburg, pp.370-375.

Vlaev, SD, Tsibrasnka, I, Dzhonova, D, Georgiev, D 2016, Preconditions of separations in STR with integrated membrane for energy-saving by recovery of value-added materials, *Machines Technologies Materials*, X , Iss. 9, pp. 22-25.

Wang, P, Cui, Y, Ge, Q, Fern, T, Chung, T 2015, Evaluation of hydroacid complex in the forward osmosis–membrane distillation (FO–MD) system for desalination, *J. Membr. Sci.*, 494, pp.1–7.

Wei, P, Cheng, L-H, Zhang, L, Xu, X-H, Chen, H-L, Gao, C-J 2014, A review of membrane technology for bioethanol production, *Renewable and Sustainable Energy Reviews*, vol. 30, pp. 388–400.

Wibisono, Y, Cornelissen, ER., Kemperman, AJB., Van der Meer, WGJ, Nijmeijer, K 2014, Two-phase flow in membrane processes: A technology with a future, *Journal of Membrane Science*, 453, pp. 566-602.

Yang, J 2013, *Prospects for flux enhancement in anaerobic membrane bioreactors treating saline wastewater*, TU Delft.

Yangali-Quintanilla, V, Maeng, SK, Fujioka, T, Kennedy, M, Amy G 2010, Proposing nanofiltration as acceptable barrier for organic contaminants in water reuse, *Journal of Membrane Science* 362, p. 334.